

# Applicability of diffraction elastic constants to rationalize anisotropic broadening of X-ray diffraction line profiles from deformed metals

Debtanu Ghosh<sup>1</sup>, Sujay Munshi<sup>2</sup>, Apurba Kanti Deb<sup>2</sup>, Partha Chatterjee<sup>1\*</sup>

<sup>1</sup>Department of Physics, Vivekananda Mahavidyalaya, Haripal, Hooghly, West Bengal, India.

<sup>2</sup>Department of Physics, Raiganj University, Raiganj, West Bengal, India.

\*Corresponding author: drchatterjee@yahoo.co.in

Received 9 October 2022; Accepted 1 December 2022; Published online 4 December 2022

## Abstract:

A simple method, to rationalize anisotropic X-ray line widths of deformed FCC metallic samples is presented. The method is based on normalized Diffraction Elastic Constant ratio (DECR) within the framework of Stokes Wilson approximation and Gaussian microstrain distribution. The observed dispersion in classical Williamson-Hall plot was significantly reduced if DECR based correction was applied to the integral breadths. Classical grain interaction models such as the Reuss and Reuss-Voigt average (Neerfeld-Hill) models were used to calculate the elastic constants of deformed polycrystals of Aluminium and Copper. It is observed that if non-uniform microstrains are present in the sample (mostly in the case of dislocated crystals) then the Reuss model is more appropriate than the Reuss-Voigt average model and is observed in the case of filed or ball-milled samples of Cu and Al. The non-linearity in the anisotropy corrected Williamson-Hall is indicative of line widening caused by the dislocation.

**Keywords:** X-ray diffraction; Microstrain broadening; Diffraction elastic constant; Williamson-Hall

## 1. Introduction

The experimental X-ray diffraction line profile is the result of the convolution of several components such as instrumental line profile due to the finite slit systems, X-ray emission profile etc. and the different sample-related microstructural contributions, such as small coherently diffracting crystallites or domains, lattice microstrains, planar or line defects, compositional inhomogeneity to name a few [1].

Different methods are used to determine such microstructural parameters. The separation of crystallite size and microstrain broadening are based on the classical method of Warren-Averbach [2, 3] based on rigorous Fourier transform of the X-ray line profiles, or on the methods of simple integral breadth methods such as Williamson-Hall [4] or Halder-Wagner [5] method. All the methods have their advantages and disadvantages. The methods based on integral breadths though approximate are used extensively for rapid analysis of XRD profiles in the field of materials science and metallurgy.

In general, it is observed experimentally that neither the

Fourier coefficients for different values of Fourier lengths/coherence length ( $L$ ) nor the widths of the diffraction lines (viz. FWHM, integral breadth etc.), are monotonic increasing functions of the diffraction vector  $d^*$  ( $= 1/d$ , where  $d$  is the distance between the respective planes of a particular reflection  $hkl$ ) [6, 7]. The phenomenon aptly known as anisotropic peak broadening may be due to anisotropic crystallite shape, planar faults or anisotropic micro-strain broadening due to grain to grain variation of lattice parameter and/or dislocations-like defects present in the material. In the case of the anisotropic crystallite size broadening the broadening depends locally on the diffraction vector but not globally on the latter. On the other hand anisotropic microstrain broadening depends globally on the diffraction vector. This communication is limited to the study of the anisotropic microstrain broadening.

In deformed materials both elastic and plastic strain may be present. It is possible to analyze both the elastic and the plastic components of the lattice strain that occurs during the deformation [8–16]. Diffraction from crystalline materi-

als is sensitive to the elastic deformation field, whether long range (pseudo-macro) or local (inhomogeneous) and gives visible effects of shift and broadening of the peak profile. As early as 1944 Stokes and Wilson [8] observed that the anisotropy of the breadths of X-ray diffraction lines generated by aggregates of distorted crystals or cold-worked metals, has a direct connection with anisotropic elastic constants. In the presence of simultaneous broadening due to small crystallite size and lattice distortion, common methods for separating size and strain effects (viz. Williamson-Hall (WH) method/Warren-Averbach (WA) method) show large deviations due to strain anisotropy and all diffraction peaks cannot be used simultaneously to extract meaningful and unambiguous information. In the absence of higher orders of a specific  $hkl$  plane approximate values of domain size and microstrain are calculated from a single diffraction peak. On the other hand the anisotropic X-ray diffraction line broadening often leads to difficulties when whole pattern fitting methods (viz. Rietveld method) are applied to the diffraction pattern of materials with even simplest cubic symmetry. Stephens [17] proposed a method to correct for this anisotropy based on lattice metric parameter and their distribution within a sample. The method was called phenomenological because it provided reasonable fits of the diffraction data, although it could not predict the true value of microstrain. Popa [18] proposed a similar variant of Stephen's model. Both the methods are widely used in Rietveld refinement or Whole Pattern fitting algorithm [19,20]. However, the methods are generally used to improve profile modeling and thus obtain reliable estimates of structural parameters.

Apart from the phenomenological approach described earlier Ungar and Borbely [7] proposed the modified Williamson-Hall and modified Warren-Averbach method to correct the observed line broadening anisotropy of dislocated crystals. The method is based on a dislocation model (more specifically the Restrictedly Random Dislocation distribution model [21] and assumes that the mean-square lattice microstrain ( $\langle \epsilon^2 \rangle$ ) averaged over all the slip systems is a function of the dislocation density ( $\rho$ ) and 'contrast' ( $C_{hkl}$ ) factor which describes the visibility of dislocations in a diffraction experiment). The rigorous assumptions involved i.e. texture free sample, equally activated slip systems limit the practical applications of the modified WH and WA methods. Ungar and coworkers subsequently developed a whole pattern fitting algorithm (MWP/CMWP) [22, 23] based on the same theoretical formulation.

The use of  $hkl$  specific Diffraction Elastic Constant (DEC) or more specifically Young's modulus ( $E_{hkl}$ ) to rationalize the anisotropic strain observed in WH plots dates back to about 1944 [8, 24, 25]. But those approaches were not widely used. Recently there has been a renewed interest in analyzing diffraction line broadening due to both elastic and plastic deformation using DEC [16, 26–28]. Wong and Dawson [27] applied the ratio of  $E_{111}$  and  $E_{100}$  to model the anisotropic elastic-plastic transition of face centered cubic (FCC) poly-crystals under uni-axial tensile loading. Zhao and Zhang adopted a similar approach [26] for deformed nano-Ni samples. Takaki et al. [28] and Jiang et al. [16],

however, used a different normalization constant.

It has recently been shown that [29, 30] elastic loading of bulk materials can also lead to peak broadening due to anisotropic stress distribution in diffracting crystallites. Elastic grain interaction models such as Voigt, [31] Reuss, [32] Neerfeld-Hill, [33, 34] Eselby-Kroner [35, 36] etc. are frequently used for the calculation of stress in deformed bulk materials. The elastic strain calculated from the diffraction peak positions and local stress is related by the X-ray elastic constants XEC ( $S_1$  and  $S_2$ ) [37]. Voigt and Reuss models represent the classical extremes of the elastic constants. Experimentally observed elastic constants are generally intermediate to them. The observed line broadening due to elastic loading is dependent on the grain-interaction model chosen.

In view of the above, in this communication, both DEC ratio and XEC ratio have been used according to the quasi elasto-plastic method suggested by Jiang et al. [16] to rationalize the broadening anisotropy observed in the linear version of the Williamson-Hall plot of plastically deformed materials. However, the method devised in this work is based on the assumption of the Stokes-Wilson approximation with an isotropic microstress distribution and a Gaussian microstrain distribution. The method has been shown to be applicable to plastically deformed materials of the FCC type. The effect of the grain interaction model, i.e. the Reuss and Reuss-Voigt (Neerfeld-Hill) average on the broadening of the diffraction line is also evaluated to determine the effective interaction of the grains. The method is applied to two model systems of deformed Copper and Aluminium. The systems thus chosen show different Zener anisotropic parameter  $A$  (defined as  $= 2(s_{11}-s_{12})/s_{44}$ , where  $s_{ij}$  are single crystal elastic constants).

The method is relatively simple and can easily quantify the strain anisotropy in plastically deformed materials based on an elasto-plastic model. This approach can effectively overcome the complexities and assumptions associated with the dislocation model based mWH/mWAmethod [7, 21] which is only applicable to dislocation induced line broadening.

## 2. Theoretical background

### 2.1 Conventional Williamson–Hall (cW-H) equation (Isotropic size-strain broadening independent of crystallographic direction)

The broadening of the XRD line profile due to small isotropic crystallites or lattice microstrain is mathematically expressed by either the Scherrer equation or Wilson formula respectively [1, 4, 38]. If both the sources of broadening is present in the sample, simplifying assumptions are often required to separate their effect. When both size and strain broadened profiles are assumed to be Cauchy a linear additive version is proposed whereas for a Gaussian approximation a quadratic additive version is proposed [1, 4] as described below.

$$\beta^* = \alpha + 2\epsilon d^* \quad (1)$$

$$\beta^{*2} = \alpha^2 + (2\epsilon d^*)^2 \quad (2)$$

Here  $\beta^* = (\beta_{\text{total}} \cos \theta) / \lambda$ , and  $d^* = 2 \sin \theta / \lambda$  and  $\alpha$  is related to the volume weighted crystallite size  $D$ . A conven-

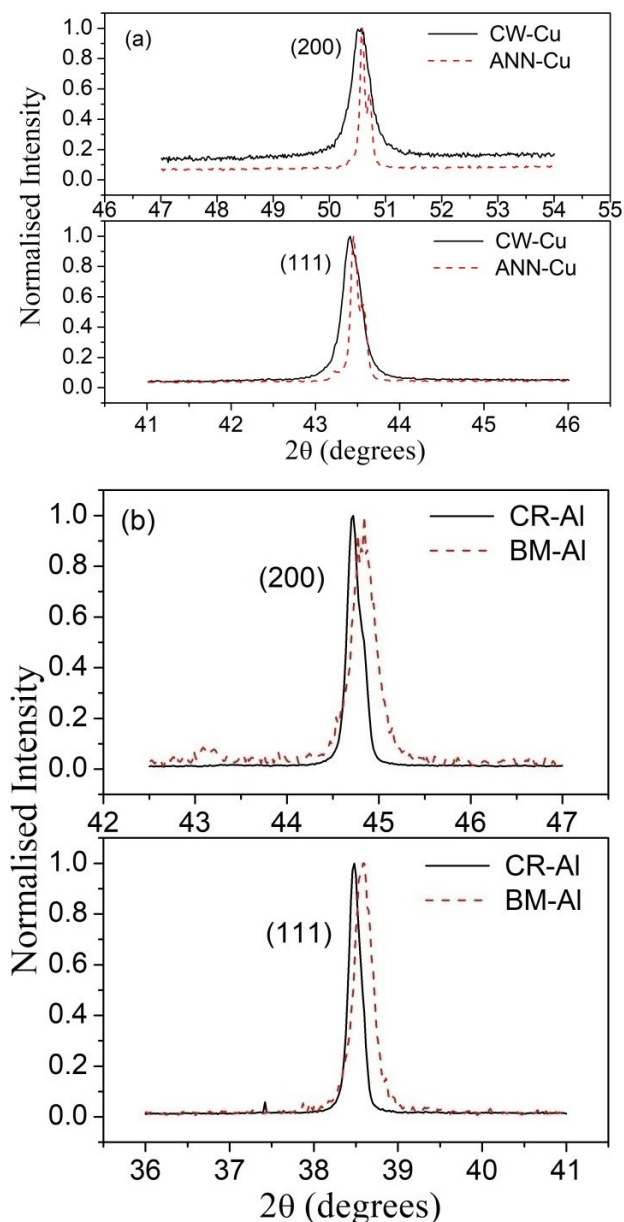


**Figure 1.** Normalised XRD pattern showing (111) and (200) peak for (a) cold-worked Cu and (b) cold-rolled and ball-milled Al samples.

tional W-H plot according to the above equations 1 or 2 for several diffraction orders gives the value of microstrain  $\epsilon$  from the slope and crystallite size  $D$  from the intercept.

## 2.2 Anisotropic microstrain broadening

The above equations predict that the x-ray line broadening is a monotonic function of  $d^*$ . Stokes and Wilson [8] identified two specific cases for the observed anisotropy in the x-ray diffraction pattern. In the first case it was considered that the material is broken down into small crystallites with different mean lattice parameters in the crystallites and in the second case distortions are assumed to be present in the crystallites. In the first case either uniform expansion or contraction is present, whereas, in the second case non-uniform expansion and contraction is allowed. The apparent strain  $\epsilon$  can either

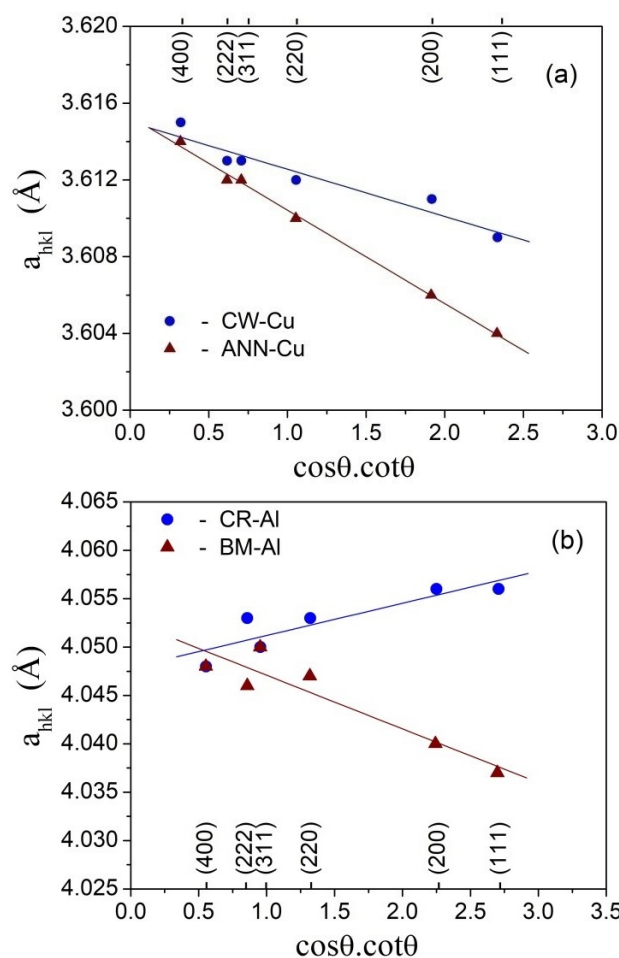


**Figure 2.** Variation of Lattice parameter ( $a_{hkl}$ ) as a function of  $\cos \theta \cot \theta$  for (a) deformed and annealed Cu-specimen and (b) cold-rolled and ball-milled Al-specimen.

be defined as the maximum strain  $\epsilon_{max}$  or *rms* strain  $\epsilon_{rms}$ . Stokes and Wilson [8] further showed that if the apparent strain  $\epsilon$  is distributed according to a Gaussian function, then for a spherically symmetric stress distribution the root mean squared strain ( $\epsilon_{rms}^2$ ) is related to mean stresses and elastic constants of the material and is given by the following equation.

$$\langle \epsilon_{rms} \rangle^2 = A + B\Gamma \quad (3)$$

Here the constants  $A$  and  $B$  depend on the elastic constants and mean square stresses and  $\Gamma = (h^2k^2 + k^2l^2 + l^2h^2)/(h^2 + k^2 + l^2)^2$  is defined as the orientation parameter for cubic crystals. Thus the microstrain determined from XRD analysis using the equations 1 and/or 2 is dependent on the crystallographic direction and the elastic constants of the deformed material.

If on the other hand, it is assumed that all values of apparent strain between 0 and a maximum value  $\epsilon_{max}$  is equally likely, then Stokes and Wilson reached the following conclusion regarding the variation of  $\epsilon_{max}$  (equation 19 of Stokes and Wilson [8]) with the orientation parameter  $\Gamma$ .

$$\epsilon_{max} = A + B\Gamma \quad (4)$$

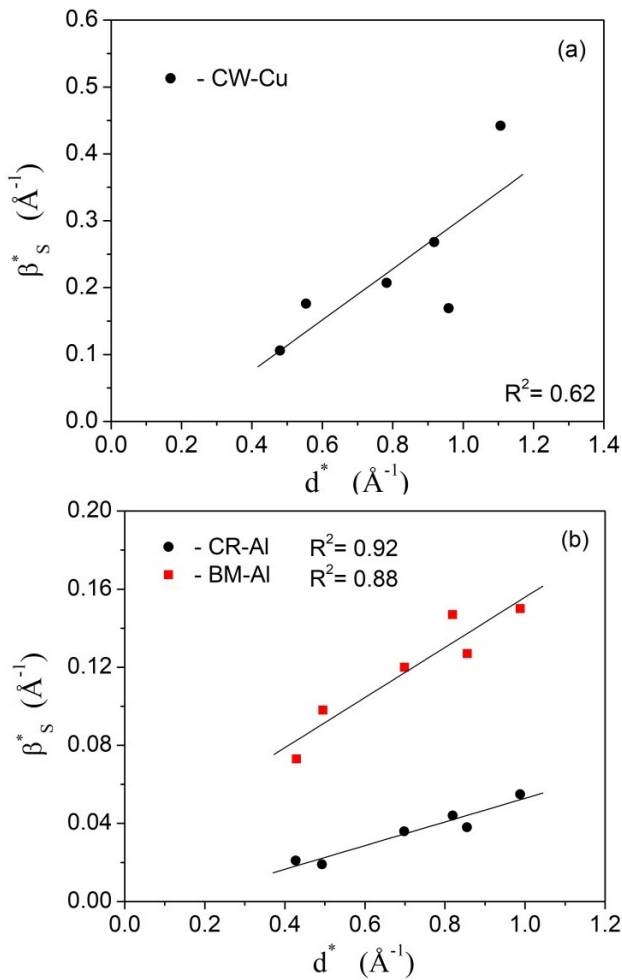


**Figure 3.** Conventional W-H plot of (a) cold worked Cu (b) deformed Al samples. Effect of stacking fault has been corrected using equation 21.

They suggested that both the equations 3 and 4 are equally likely in describing the anisotropic line broadening in X-ray diffraction pattern.

Substituting equation 3 and 4 into equation 1 the following expressions are derived.

$$\beta^* = \alpha + 2(A + B\Gamma)^{\frac{1}{2}} d^* \quad (5)$$

and

$$\beta^* = \alpha + 2(A + B\Gamma) d^* \quad (6)$$

Either of the above two equations can be used as a generalized Williamson-Hall plot if the constants  $A$  and  $B$  are either known or assumed according to a grain-interaction model. It has been argued [8, 17] that equation 5 is more applicable. The usable forms of the above equations are discussed in the following sections.

The equations 5 and 6 indicate that scaling of anisotropic X-ray line broadening is possible by using elastic constants. Ungar and Borbely [7] earlier focused on the method by introducing the contrast factor  $C_{hkl}$  as a function of the Miller indices  $hkl$  only for the correction of anisotropy in WH plot or Fourier coefficients prevalent in dislocated crystals. They proposed that the mean square strain  $\langle \epsilon_{L,d^*}^2 \rangle$  can be

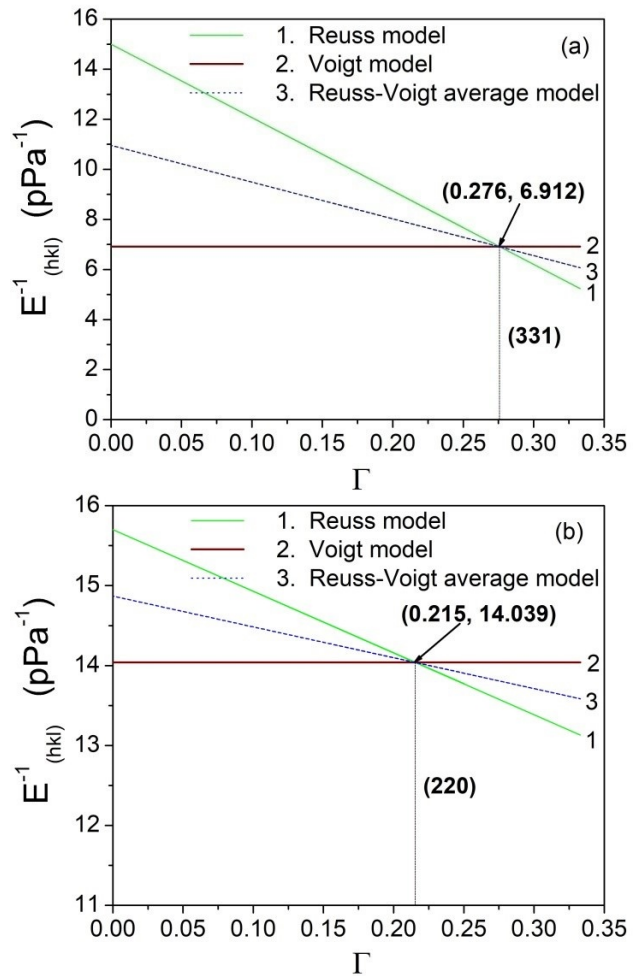


**Figure 4.** Relation between the orientation parameter  $\Gamma$  and the reciprocal of  $hkl$ -dependent Young's modulus  $E_{hkl}$  of (a) and (b) Al for R, V and R-V models.

decoupled in terms of the Fourier length  $L$  and diffraction order according to the relation [39].

$$\langle \epsilon_{L,d^*}^2 \rangle = \langle \epsilon_L^2 \rangle C_{hkl} \quad (7)$$

The diffraction order dependence is absorbed in the term  $C_{hkl}$ . It was further shown [40] that the contrast factor can be expressed in the form

$$C_{hkl} = \hat{A} + \hat{B}\Gamma \quad (8)$$

here  $\hat{A}$  and  $\hat{B}$  depend on the elastic constant and the type of dislocation present in the material.

### 2.3 Diffraction-specific elastic constants

Diffraction elastic constants are routinely used for the determination of stress in crystalline materials. There are several grain-interaction models which provide an outline for the calculation of stress and strain as a function of crystallographic orientation of a crystal in an elastically deformed specimen. For such analysis knowledge of the diffraction-specific Young's modulus  $E_{hkl}$  and Poisson's ratio  $\nu_{hkl}$  or X-ray elastic constants  $S_1$  and  $1/2S_2$  are used [37, 41, 42]. The two classical approaches of Voigt [31] and Reuss [32] grain-interaction models are used for describing the isotropic

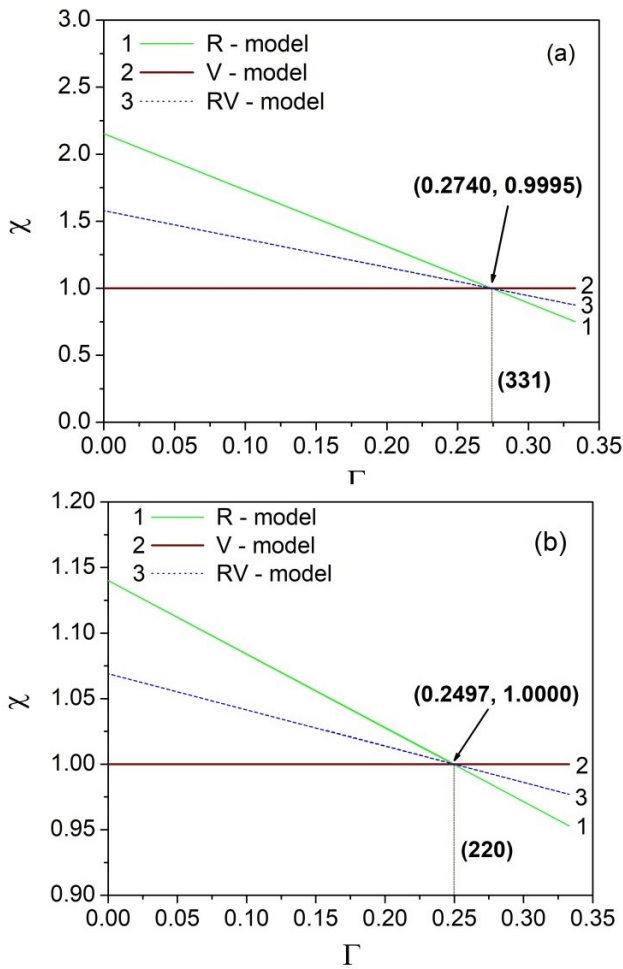


**Figure 5.** Plot of Diffraction Elastic Constant ratio  $\chi$  with orientation factor  $\Gamma$  for (a) FCC Cu, where  $E_{hkl}$  was normalized in (331) direction and (b) FCC Al, where  $E_{hkl}$  was normalized in (220) direction.

elastic behaviour of grains within a polycrystal under elastic loading. However, effective grain-interaction models, such as the Neerfeld–Hill [33, 34] model, uses a linear combination of the extreme Voigt and Reuss models, and thus yield results which compares well with the experimental observations.

In the Voigt model the strain tensor is same for all crystallites implying that different crystallites have different stress tensors. In cubic crystal systems, the reciprocal of  $hkl$ -dependent Young’s modulus ( $1/E_{hkl}$ ) of single crystals or polycrystalline materials follows the standard formula [37, 42].

$$\frac{1}{E_{hkl}^V} = \frac{2S_{11}(S_{11} + S_{12} + 2S_{44}) - 2S_{12}(2S_{12} + S_{44})}{S_{44} + 6(S_{11} - S_{12})} \quad (9)$$

Similarly the X-ray elastic constants (XEC) are expressed as

$$S_1 = \frac{2S_0(s_{11} + 2s_{12}) + 5s_{12}s_{44}}{6s_0 + 5s_{44}}, \quad \frac{1}{2}S_2 = \frac{5(s_{11} - s_{12})}{6s_0 + 5s_{44}} \quad (10)$$

with  $s_0 = s_{11} - s_{12} - s_{44}/2$ .

In the Reuss model on the other hand the stress distribution

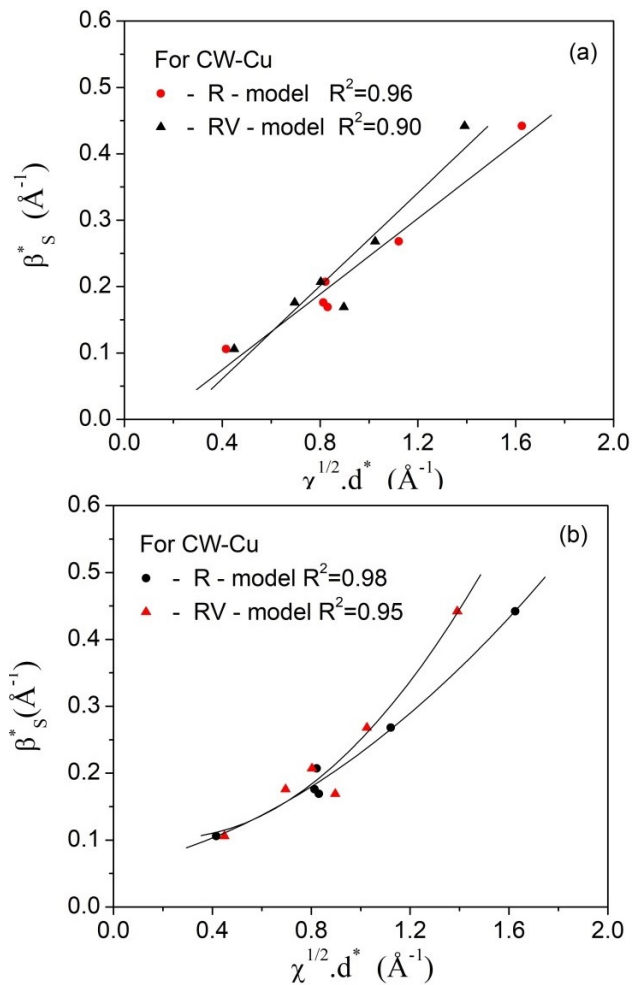


**Figure 6.** Anisotropy corrected Williamson-Hall plot for Copper sample (a) linear fit and (b) quadratic fit.

is isotropic and the strain tensor is different for different crystallites leading to the following expressions for  $E_{hkl}$ ,  $S_1$  and  $S_2$  [37, 42].

$$\frac{1}{E_{hkl}^R} = s_{11} - (2s_{11} - 2s_{12} - s_{44})\Gamma \quad (11)$$

$$S_1^{hkl} = s_{12} + s_0\Gamma, \quad \text{and} \quad \frac{1}{2}S_2^{hkl} = s_{11} - s_{12} - 3s_0\Gamma \quad (12)$$

The Voigt model (equal strain tensor) and the Reuss model (equal stress tensor) thus yield the lower and upper limit of elastic constants respectively. It was shown that (e.g. Neerfeld, Hill, Welzel et al.) [33, 34, 37] that neither of the models viz. Voigt or Reuss is compatible with the behavior of the real polycrystals. It was suggested that the effective diffraction elastic constants are arithmetic averages of the values as obtained from Reuss and Voigt model and is expressed as

$$\left(\frac{1}{E_{hkl}}\right)^{eff} = \frac{1}{2}\left(\frac{1}{E_{hkl}^R} + \frac{1}{E_{hkl}^V}\right) \quad (13)$$

#### 2.4 The diffraction elastic constant (DEC) $\chi$

The equations 5 and 6 suggest that the X-ray line broadening due to microstrain scales with the elastic constants. In

**Table 1.** Single crystal elastic compliance data of Aluminium and Copper [42]

Sample	$s_{11} \times 10^{11}$ Pa <sup>-1</sup>	$s_{12} \times 10^{11}$ Pa <sup>-1</sup>	$s_{44} \times 10^{11}$ Pa <sup>-1</sup>	A
Al	1.57	-0.57	3.51	1.219
Cu	1.5	-0.63	1.33	3.203

general, it is accepted that lattice strain produces anisotropic displacements of the atoms with respect to their reference lattice positions and produces anisotropic X-ray diffraction line broadening. The average strain level can be calculated on the basis of mean field or uniform deformation model, as generally accepted in crystal plasticity models. In the present work it has been considered that plastic lattice strain broadening results in accordance to  $hkl$ -independent stress distribution function ( $\sigma$ ) or the uniform deformation model in the light of Stokes–Wilson approximation.

Jiang et al. [16] introduced the  $hkl$  dependent diffraction Young's modulus ratio  $\chi$  as

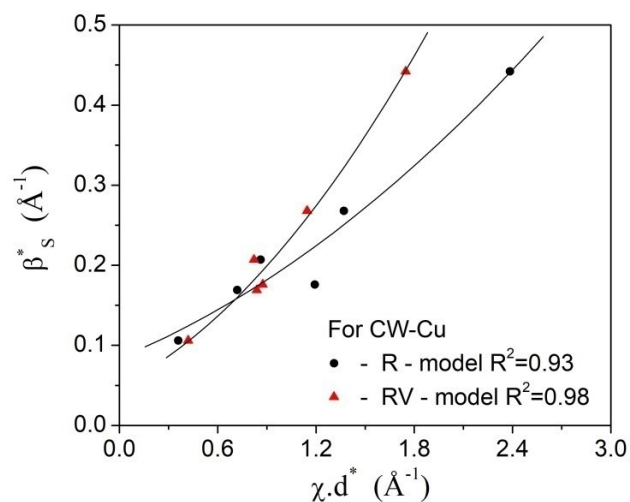
$$\chi = \frac{E_0}{E_{hkl}} \quad (14)$$

where  $E_0$  is the elastic constant of a reference reflection (Jiang et al. [16] assumed  $E_0 = E_{331}$ ). It is possible to decouple the diffraction order dependent component of the lattice microstrain using equation 14. Using elasticity theory the maximum value of microstrain can be expressed as

$$\epsilon_{hkl}^{max} = \frac{\sigma}{E_{hkl}} = \frac{\sigma}{E_0} \times \frac{E_0}{E_{hkl}} = \chi \epsilon_0 \quad (15)$$

The value  $\epsilon_0$  refers to the true or order-independent component of the lattice microstrain and the order dependent part is collected in the value of  $\chi$ .

However, in the presence of a microstrain distribution in the sample and if further the distribution function is exactly

**Figure 7.** Anisotropy corrected Williamson-Hall plot for Cu sample using equation 17.

Gaussian in nature, then it is assumed that the equations 3 and 7 are identical and differ only with respect to the constants. Assuming that this expression holds in general using equation 3, 7, 14 and 15, equation 5 and 6 can be written as

$$\beta^* = \alpha + 2\sqrt{\chi}\epsilon_0^{rms}d^* \quad (16)$$

or

$$\beta^* = \alpha + 2\chi\epsilon_0^{max}d^* \quad (17)$$

Here  $\epsilon_0^{rms}$  (or  $\epsilon_0^{max}$ ) is the lattice microstrain of the assumed reference reflection ( $hkl$ ) for both samples. Equations 16 and 17 can thus be termed as generalized Williamson-Hall plot.

### 2.5 X-ray elastic constant ratio $m_{hkl}$

The X-ray elastic constant  $S_{hkl}$  is routinely used for the determination of stress in polycrystalline samples. In the present communication it is proposed to use  $S_{hkl}$  for improving the linearity of WH plot and is shown that the X-ray elastic constants can be used for meaningful determination of lattice microstrain. X-ray elastic constant is defined by the relation  $S_{hkl} = \nu_{hkl}/E_{hkl}$ , where  $\nu_{hkl}$  is the Poisson's ratio. In the present work,  $m_{hkl}$  has been defined by normalizing the  $hkl$ -dependent X-ray elastic constant with respect to a standard  $S_0$ . Reuss and Reuss-Voigt average models are used to calculate the X-ray elastic constants. The anisotropic plastic strain  $\epsilon_{hkl}^{Pla}$  is expressed as following,

$$\epsilon_{hkl}^{Pla} = \frac{\sigma}{E_{hkl}} = \frac{\sigma}{E_0} \times \frac{E_0}{E_{hkl}} = \frac{\sigma}{E_0} \times \frac{\nu_{hkl} \cdot E_{hkl}^{-1}}{\nu_{hkl} \cdot E_0^{-1}} = \epsilon^{Pla*} \times \frac{S_{hkl}}{S_0} = \epsilon^{Pla*} \times m_{hkl} \quad (18)$$

$S_0$  is the XEC constant of a reference  $hkl$  reflection. Using this formalism WH equation can be written as

$$\beta^* = \alpha + 2 \cdot \epsilon^{Pla*} \cdot m_{hkl} \cdot d^* \quad (19)$$

## 3. Experimental procedure and method of analysis

Commercial purity Al samples was cold-rolled to 80% thickness reduction at room temperature corresponding to true strain of 1.61 ( $e = \ln(d_0/d)$ , where  $d_0$  and  $d$  denotes the initial and final thickness). The XRD pattern of cold-rolled Al samples (CR-Al) was recorded in the TD-RD plane. Cold-worked copper specimen was prepared by hand filing. The filed powder was annealed at 500°C for 10 hours to remove the effect of plastic deformation. Commercial purity Al powder was ball-milled in a Fritsch Pulverisette planetary mill (P5) operating at 300 rpm for 8 hrs. Zirconia milling media (balls and vials) with ball to powder ratio of 1:10 was employed for the purpose of milling.

The X-ray diffraction pattern of all samples as well as the standard Si powder (for instrumental broadening correction) were taken at room temperature in a X'Pert PRO diffractometer (PW 3040/60, PANalytical) using Ni-filtered Cu  $K_\alpha$  radiation. A fixed divergence slit of opening 1° and a receiving slit of opening 0.1 mm were used for data collection. A step width of 0.02° and a counting time of 10 s per

**Table 2.** Calculated values of diffraction specific elastic constants. The values  $E_{hkl}$  and  $\nu_{hkl}$  represents the  $hkl$  specific values of Young's modulus and Poisson's ratio respectively. The superscripts  $R$  and  $V$  correspond to Reuss and Voigt elastic grain interaction models respectively.

Parameters(in Gpa)	Copper	Aluminium
$E_{111}^R$ and $E_{222}^R$	191.1	76.1
$E_{200}^R$ and $E_{400}^R$	66.7	63.7
$E_{220}^R$	130.3	72.6
$E_{311}^R$	96.2	69.0
$E^V$	144.7	71.3
$\nu_{111}^R$ and $\nu_{222}^R$	0.27	0.34
$\nu_{200}^R$ and $\nu_{400}^R$	0.42	0.36
$\nu_{220}^R$	0.34	0.34
$\nu_{311}^R$	0.38	0.35
$\nu^V$	0.32	0.35

step were used.

The X-ray diffraction line profiles for each specimen were fitted using the software WinPLOTR [43] employing a modified-Thomson-Cox Hastings (TCHZ) profile fitting function [44]. Instrumental broadening correction was done according the method suggested by deKeijsers et al. [45].

The single crystal elastic constants for Copper and Aluminium are obtained from the literature [42] and the corresponding diffraction specific elastic constants has been calculated and are collected in Tables 1 and 2.

By using the above values, the values of  $S_{hkl}$  for  $R$  and  $R$ - $V$  model can be easily calculated.

## 4. Results and discussions

### 4.1 Lattice parameter and stacking fault analysis

Figure 1 shows a part of the diffraction pattern of copper and aluminium samples. Effect of plastic deformation is evident in Cu samples from the enhanced line broadening in deformed Cu sample compared to the annealed sample of Cu. In the case of the Al samples the broadening of the ball milled samples is greater compared to the cold-rolled samples indicating either enhanced crystallite size and/or reduced lattice strain for the latter. It is further observed that there is a small peak shift which may be due to change in lattice parameter, presence of stacking faults and long range residual stresses in the deformed material.

Figure 2 shows the variation of  $a_{hkl}$  as a function of  $\cos \theta \cot \theta$  for the Copper and Aluminium samples. It has been shown that [46] the calculated values of lattice param-

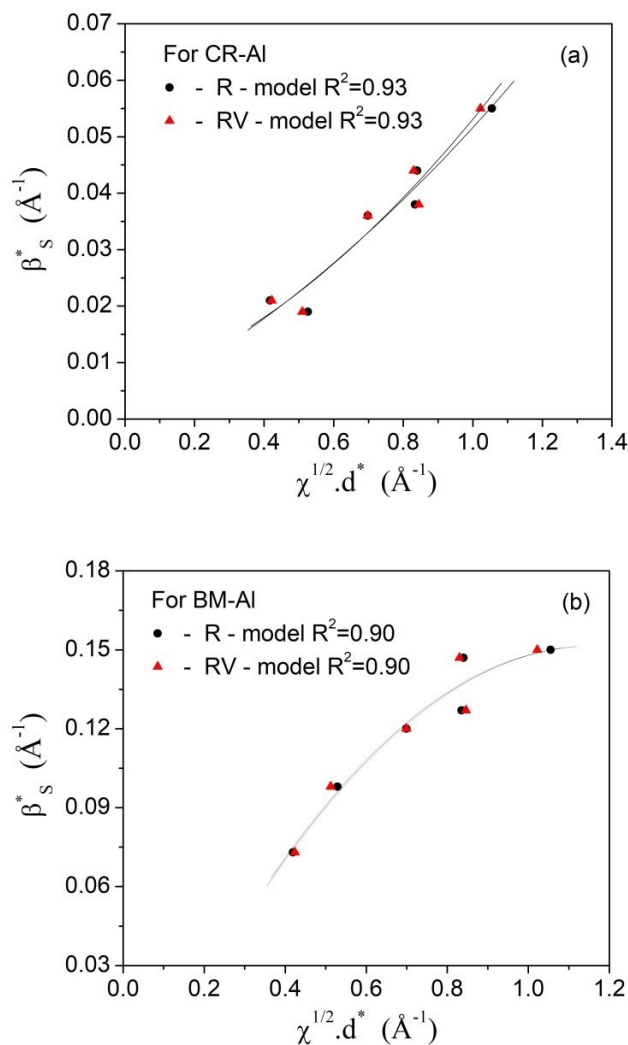


**Figure 8.** Anisotropy corrected generalized Williamson-Hall plot for (a) cold-rolled Aluminium (CR-AI) and (b) ball-milled Aluminium (BM-AI) samples.

eter of annealed samples usually follows a smooth straight line when plotted as a function of  $F(\theta) = \cos \theta \cot \theta$ . This feature is evident from Figure 1(a) for the annealed Cu sample. The true lattice parameters obtained by the extrapolation to  $\cos \theta \cot \theta$  are given in Table 3 for all the samples. The values of lattice parameter of Cu and Al are consistent with the literature values of  $a_{Cu} = 3.615 \text{ \AA}$  (PDF card no 89-2838) and  $a_{Al} = 4.049 \text{ \AA}$  (PDF card no 85-1327). It may be mentioned here that the slope of the plot of lattice parameter for cold-rolled Al is different from the other samples. This is probably due to small specimen displacement which occurred when the bulk CR-AI sample was placed in the sample holder. The value of the lattice parameter of the BM-AI sample is slightly higher than the true lattice parameter of Al. This small change in the lattice parameter in ball milled samples is common and is often attributed to disorder in the grain boundary regions.

It is well known that the X-ray diffraction peaks of deformed FCC crystals are shifted from the peak positions of the un-deformed crystals due to a composite effect of the existence of stacking faults and long range residual stress

**Table 3.** Lattice parameter and deformation stacking fault probability values of deformed samples.

Specimen	Lattice parameter $a_0$ (nm)	Stacking Fault probability $\alpha$ (%)	Change in lattice parameter $\Delta a/a_0$	Residual stress $\sigma$ (Mpa)
Cold-worked copper	0.3615	0.3	-0.0003	11
Annealed copper	0.3615	-	-	-
Cold-rolled Aluminium	0.4048	0.1	-0.0001	88
Ball milled Aluminium	0.4053	0.02	0.0004	-71

present in the material [2, 46]. In the present work it is assumed that in addition to faulting, long range residual strain ( $\epsilon_L$ ) and the fractional change of lattice parameter  $\Delta a/a_0$  also shifts the position of diffraction profile. Assuming that the residual strains are produced by residual stress  $\sigma$ , the residual strain is expressed as  $\langle \epsilon \rangle = (S_1)_{hkl} \sigma$ , where  $(S_1)_{hkl} [= (S_1^V + S_1^R)/2]$  is the arithmetic average of X-ray elastic constant. The superscripts  $V$  and  $R$  correspond to Voigt and Reuss grain interaction models respectively. Taking all these into consideration the peak shift can be written in terms of  $2\theta$  as

$$(\Delta 2\theta_{hkl}) = -\frac{360}{\pi} \left\{ \frac{\Delta a}{a_0} + (S_1)_{hkl} \sigma + G_{hkl} \alpha \right\} \tan \theta \quad (20)$$

The values of  $\Delta a/a_0$ ,  $\sigma$  and  $\alpha$  can be obtained from the above relation from the measured value of peak shifts ( $\Delta 2\theta_{hkl}$ ) for different  $hkl$  reflections of the deformed and well annealed material. In order to avoid the error in measuring precisely the peak position the difference in the separation of peaks of indices  $hkl$  and  $h'k'l'$  are usually measured for the deformed and annealed samples. The faulting coefficients  $G_{hkl}$  are calculated according to (Warren 1969) [2]. The result of peak shift analysis for the (111 - 200) and (222 - 400) profile pairs are collected in Table 3. It is observed that cold-worked Cu specimen shows slightly higher stacking fault probability compared to deformed Al specimen in accordance to the fact that the stacking fault energy of Cu is less than that of Al. Residual stresses are present in the samples of cold-rolled Al and ball milled Al. Long range residual stresses present in the cold-rolled Al samples can explain the diffraction peak shifts observed in Fig 2.

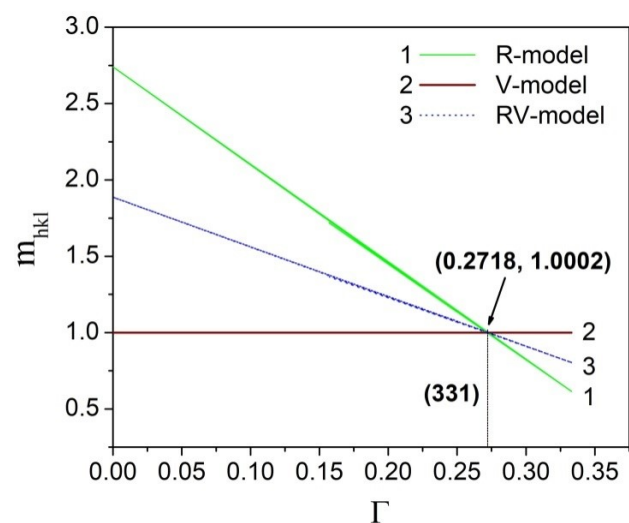
#### 4.2 Conventional williamson hall plot

Warren [2] has shown that when stacking and twin faults are present in the material the apparent particle/crystallite size is smaller than the 'true' particle size. If  $\alpha$  and  $\beta$  are the stacking and twin fault probabilities respectively, the reciprocal of the crystallite size increases by an amount of  $(1.5\alpha + \beta)W(d^*)/a$  where  $W(d^*)$  is diffraction order specific constant. Ungar, Revesz and Borbely [47] showed that the effect of stacking and/or twin fault broadening in the classical WH plot can be corrected according to the equation

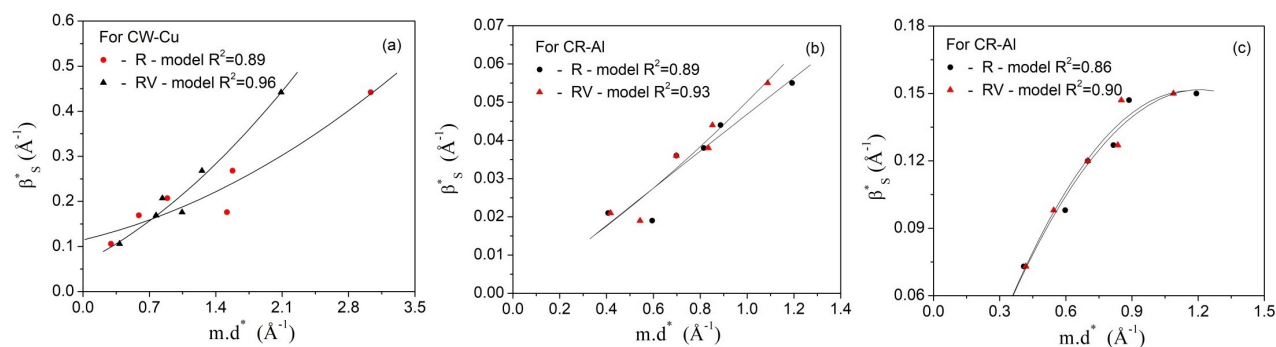
$$\beta_{corr} = \beta_{total} - (1.5\alpha + \beta)W(d^*)/a \quad (21)$$

Figure 3(a) shows a conventional linear version of WH-plot for cold-worked Cu-sample after correction for peak broadening due to stacking fault. Figure 3(b) shows the corresponding c-WH plot for cold-rolled Al (CR-Al) and

ball-milled Al (BM-Al). The scatter of the points about the average line indicates anisotropic line broadening. The correlation coefficients  $R^2$  are included in the graphs. The value of  $R^2$  is much lower for CW-Cu sample compared to CR-Al or BM-Al samples indicating that elastic anisotropy has a profound influence on the observed X-ray line broadening. The average line fitted to the data gives a negative value of the intercept for the CW-Cu sample, indicating an unrealistic value of volume weighted crystallite size. However, taking into account the pair of orders (111) - (222) and (200) - (400) the values of lattice microstrain is obtained to be  $\epsilon_{\langle 111 \rangle} = 0.001$  and  $\epsilon_{\langle 100 \rangle} = 0.004$ . This indicates that the microstrain is anisotropic in nature and is maximum along [100] direction and minimum along [111] direction. If one imagines that this anisotropy is due exclusively to anisotropic elasticity, as suggested by Stokes and Wilson 1944 [8], and the anisotropic microstresses ( $\sigma_{hkl}$ ) are preferentially directed along the diffraction vector then according to linear elasticity,  $\sigma_{hkl} = E_{hkl} \epsilon_{hkl}$ . The ratio of  $\epsilon_{\langle 100 \rangle} / \epsilon_{\langle 111 \rangle}$  is obtained to be 4 for CW-Cu sample. Assuming that the microstresses are independent of diffraction order the corresponding ratio for  $E_{111}/E_{100}$  is 2.9 for a Reuss grain interaction model and 1.8 for a Reuss-Voigt average (Neerfield-Hill) model. From the above result, it appears that the Reuss model is more suitable to explain the increasing anisotropy in cold-worked Cu samples.



**Figure 9.** Plot of XEC ratio  $m_{hkl}$  with orientation factor  $\Gamma$  for Reuss, Voigt and Reuss-Voigt grain interaction models for FCC Cu.



**Figure 10.** Anisotropy corrected generalized WH plot on the basis of XEC ratio  $m_{hkl}$  for (a) CW-Cu (b) CR-AL and (c) BM-AL samples.

However, the ratio of  $(\epsilon_{<100>}/\epsilon_{<111>})$  for CR-Al and BM-Al samples are 2 and 0.9 respectively and the corresponding values of  $(E_{111}/E_{200})$  are 1.2 and 1.1 for Reuss and Reuss-Voigt models respectively. This suggests that either Reuss or Reuss-Voigt average value may be sufficient for rationalizing the observed broadening anisotropy in Al-samples.

### 4.3 Orientation-dependent elastic moduli

The discussion in the previous section shows that it is possible to rationalize the observed anisotropy in the broadening of the XRD lines based on an elasto-plastic model as described by Jiang et al. [16]. However, the observed microstrain anisotropy is much higher than predicted by elastic anisotropy alone in the case of deformed Cu sample and that might be due to prominent dislocation induced microstrain broadening and/or other sources of microstrain broadening. Equation 11 clearly shows that there is a linear relationship between the reciprocal of  $hkl$ -dependent (diffraction) modulus of elasticity and the orientation parameter. This theoretical dependence is explicitly shown in Figure 4 for various grain interaction models. It can be seen from the plot that the graphs intersect at a point which indicates that for a certain value of  $\Gamma$  the value of elastic constant  $E_{hk}$  is independent of the selected model. Jiang et al. [16] use this value as a reference elastic constant  $E^*$ . The result presented in this work shows that the points of intersection are  $\Gamma = 0.276$  for Cu and  $\Gamma = 0.215$  for Al.

In practical diffraction experiment the reference Young's modulus ( $E^*$ ) for Cu or Al-sample was chosen accordingly. The value of the abscissa results in  $E^* = E_{(331)}$  for Cu (Figure 4(a)) and  $E^* = E_{(220)}$  for Al (see Figure 4(b)), which corresponds to crystallographic directions (331) and (220).

### 4.4 Correction based on diffraction young's modulus ratio $\chi_{hkl}$

The diffraction Young's modulus ratio is obtained from equation 14 using the elastic constants of (331) and (220) as a reference and is shown in Figure 5 as a function of  $\Gamma$  for FCC-Cu and Al for the Voigt, Reuss and Reuss-Voigt (Neerfeld-Hill) average models. There is a good linear relationship between the two parameters for the three models. These results show that the intersection points are  $\Gamma = 0.274$  for Cu and  $\Gamma = 0.249$  for Al. It is concluded that the intersection points are a stable region having same range,  $\Gamma =$

0.215 to 0.276 as obtained previously.

### 4.5 Correction of the W-H plots based on $\chi_{hkl}$ (generalized WH plot)

The anisotropy observed in the WH plot for the cold-worked Cu and Al samples (see Figure 3) is corrected with the anisotropy correction factor  $\chi_{hkl}$ . From equation 16 or 17 it is clear that the effective scale factor for anisotropy correction is either  $\sqrt{\chi}$  or  $\chi$  similar to that of  $\sqrt{C_{hkl}}$  for the modified WH plot [7]. Figure 6(a) shows the plot of  $\beta^*$  against  $\sqrt{\chi}d^*$  for cold-worked Cu sample for the Reuss and Reuss-Voigt average (Neerfeld-Hill) model. At this point it should be mentioned here that the Voigt model cannot be used to correct the observed anisotropy. Table 4 list the value of crystallite size and microstrain. It is clear from the plot that the anisotropy observed in the c-WH plot is substantially minimized. A better fit is observed for the Reuss model compared to the Reuss-Voigt average model. However, a straight line fit leads to a negative intercept which indicates an unrealistic value for the crystallite size. A better fit of the data is obtained for a quadratic fit of the data (see Figure 6(b)). Reliable values for size and strain can only be obtained if the data are modeled according to Reuss model. The Reuss-Voigt average model provides unrealistic values for size and strain. At this point, it should be mentioned that the modified WH plot for dislocation induced strain broadening is generally non-linear in nature [7, 39, 40]. Similar non-linear nature was observed here for the data of cold-worked copper samples. This indicates that dislocations are the main source of lattice microstrain. The  $rms$  strain ( $\epsilon_{rms}$ ) is similar ( $\sim 0.2\%$ ) for both Reuss and Reuss-Voigt model. However, the volume-weighted crystallite size varies with the model chosen. From the diagrams above, it is clear that the dispersion observed in the WH plot for cold-worked materials can only be accounted for on the basis of elastic constants and a reliable estimate of the  $rms$  value of lattice microstrain can be obtained.

It is worth comparing the results obtained in this communication with the method proposed by Jiang et al. [16]. They proposed a correction for broadening anisotropy based on equation 17, where the scaling parameter is  $\chi$  instead of  $\sqrt{\chi}$ . Figure 7 shows such a plot for cold-worked Cu and the results are summarized in Table 4. It is observed that the dispersion is minimized when the Reuss-Voigt model

**Table 4.** Crystallite size and microstrain values obtained from anisotropy corrected WH plot for Reuss and Reuss-Voigt model grain interaction models.

(All data using linear regression, ‘\*’ indicated quadratic fit, -ve crystallite size means above detection limit. *R* represents Reuss model and *RV* represents Reuss-Voigt average model.)

Anisotropy Corrected - WH plot												
From $\beta_S^* - \chi d^*$ plot				From $\beta_S^* - \sqrt{\chi} d^*$ plot				From $\beta_S^* - m. d^*$ plot				
D (nm)		$\epsilon_{max}(10^{-3})$		D (nm)		$\epsilon_{rms}(10^{-3})$		D (nm)		$\epsilon(10^{-3})$		
R	RV	R	RV	R	RV	R	RV	R	RV	R	RV	RV
CW-Cu	135	117*	0.7	1*	96*	48*	2	2.4	72	90*	1	1
	(60)	(9)	(0.1)	(0.1)	(51)	(31)	(0.1)	(0.3)	(19)	(55)	(0.1)	(0.1)
CR-Al	-ve	>10 <sup>3</sup> *	0.46	0.3*	>10 <sup>3</sup> *	>10 <sup>3</sup> *	0.4	0.4	>10 <sup>3</sup>	>10 <sup>3</sup>	0.4	0.5
			(0.04)	(0.04)			(0.04)	(0.04)			(0.05)	(0.04)
BM-Al	160	188	1	1	189	200	0.8	0.8	141	177	0.9	1
	(46)	(62)	(0.1)	(0.1)	(62)	(73)	(0.1)	(0.1)	(38)	(55)	(0.01)	(0.1)

is used compared to the Reuss model in contrast to the previous case. However, a generalized characteristic can be observed that in both cases the plot is, according to other studies, [7, 39, 40] of a non-linear nature. It has been argued that integral breadth ( $\beta^*$ ) for pure dislocation-induced micro-deformation is a pure quadratic function of  $d^*$ . However, for a strictly Gaussian strain distribution leading to random atomic displacements a linear  $\beta^* - d^*$  plot is obtained. Furthermore, the non-linearity of the plot also depends on the defect-correlation and is approximately linear if the defect correlation is weak. In the present work it was observed that the  $\beta^* - d^*$  does not show a purely quadratic dependence. It is worth comparing the data presented in this paper with the recent results on plastically deformed Cu. Most of the recent results are based on the Ungar’s method of modified-WH /modified WA and / or CMWP which are sufficiently elaborate with a large number of fitting parameters. Some of the results are collected in Table 5.

It is observed that the average dislocation density of Cu deformed by various processes (viz. ball-milling, ECAP, cold-rolling) varies markedly between  $(1 - 2) \times 10^{11} / \text{cm}^2$ . It is thus clear from the Table that although the crystallite size values differ considerably the values of lattice microstrain which varies as  $\rho^{1/2}$  is insensitive to the deformation history of the material. In the present study the  $\epsilon_{rms}$  value obtained from the  $\beta_S^* - \sqrt{\chi} d^*$  plot is used to calculate the dislocation density of deformed Cu sample using the Williamson-Smallman (WS) method and is on the order of  $1 \times 10^{11} / \text{cm}^2$ . The result obtained here compares well with the literature values as cited in Table 5. Therefore, it is obvious that the present method to correct for anisotropy in the WH method using elastic constants only provides a reliable value for microstrain and thus dislocation density values without the use of more elaborate modified WA/MWP/CMWP methods. The anisotropy corrected WH plot for cold-rolled Al (CR-AL) and ball-milled Al (BM-AL) are shown in Figure 8. It

**Table 5.** Comparison with other works [48–53].

Sample	<i>D</i> (nm)	$\epsilon$ ( $10^{-3}$ )	$\rho$ ( $10^{15}/\text{m}^2$ )	Method/Ref
ECAP Cu(1 pass)	110 $\ddagger$	-	0.91	CMWP/49
ECAP Cu	71 $\ddagger$	-	1.2	CMWP/50
CR-Cu (50%)	68 $\ddagger$	-	2.6	CMWP/51
Ball milled Cu (48 hr)	26 $\ddagger$	-	2.08	mWA/52
Ball milled Cu (48 hr)	20.9	0.15	1	WH/WS/52
CW-Cu	47	-	2.15	WA/53

is observed that in both cases both the Reuss and Reuss-Voigt average model provide identical values for crystallite size and lattice microstrain. This can also be seen in the values listed in Table 4. In the case of cold-rolled samples, the effect of crystallite size is negligible. The lattice microstrain on the other hand is greater in the case of ball-milled samples. However, it should be noted that the grain interaction model has little influence on the size-strain values. Table 4 also list the maximum strain values obtained from the plot of  $\beta_S^* - \chi d^*$  (according to equation 17) as reported by Jiang et al. [16]. The results agree with the results according to equation 16. The microstrain value for ball milled Al in the present case is of the order of 0.1% which is less than for ball-milled Al alloy ( $\sim 0.3\%$ ) [53]. Khan et al. [54] observed a grain size of  $\sim 48$  nm and a microstrain of  $\sim 0.1\%$  for Al milled for 10 hrs, which is very comparable with the results obtained in this communication. It is well established that dislocation cell structure develops in cold-rolled Al when deformed at a true strain of 0.3% [55]. In the present case the true strain is approximately 1.6%, suggesting that a finer dislocation cell structure may have been achieved. The dislocation density was found to be  $\sim 10^{11}$  /cm<sup>2</sup> [55]. Satheesh Kumar and Raghu [56] obtained a grain size of the order of 1000 nm for plastically strained Al using TEM and WH analysis, which can be well compared with the values observed here for cold-rolled Al with identical true strain. Therefore, it is thus clear that the application of diffraction elastic constant to rationalize broadening anisotropy yields reliable results and is well comparable with the results of other authors.

#### 4.6 Correction of the W-H plots based on $m_{hkl}$

This section discusses the application of x-ray elastic constants (XEC) to explain the broadening anisotropy using the method described earlier. The rationale behind the use of XEC ratio ( $m_{hkl}$ ) to correct for broadening anisotropy arises from the fact that  $m_{hkl}$  bears a linear relationship with the orientation factor  $\Gamma$ , similar to that shown Figure 5 (Figure 5 and equation 12). Figure 9 shows the variation of  $m$  with  $\Gamma$  for Cu. Similar results were obtained for Al. Figure 10 shows the plot of  $\beta - m_{hkl}d^*$  for the various samples. It is observed from Figure 10 that for the Reuss-Voigt model, the dispersion in the WH data is minimized and results in a better fit of the data compared to the Reuss model for cold-worked Cu. However, for the ball-milled and cold-rolled Al samples each of the models gives an identical result similar to that observed above. The crystallite size and microstrain values obtained from the linear fit of the data are shown in Table 4 and can be well compared with the results obtained from the  $\beta^*$  vs  $\sqrt{\chi}d^*$  plot.

Therefore, it is thus clear from the foregoing discussion that it is possible to minimize the anisotropic data spread observed in the Williamson-Hall plot by using the ratio of the diffraction elastic constants  $E_{hkl}$  or  $S_{hkl}$ . However, a possible uncertainty regarding the choice of the grain interaction models cannot be ruled out. For example, in cold-worked Cu sample the results of  $\beta^*$  versus  $\sqrt{\chi}d^*$  agree with the Reuss model, while the results of  $\beta^*$  versus  $\sqrt{\chi}d^*$  are more consistent with Reuss-Voigt average model. A possible

reason for this discrepancy is likely to be related to the underlying assumptions in the two cases. In the first case, non-uniform strains are allowed in the crystallites, while in the second case the strain in the crystallites is assumed to be constant. It seems that the first assumption is better for deformed powder materials and  $\beta^*$  versus  $\sqrt{\chi}d^*$  plot is more appropriate. For the deformed Al samples, at least in the present case, each of the methods provides a reliable result.

## 5. Conclusion

A simple method is presented to correct for anisotropic X-ray line broadening. The method is based on the diffraction specific elastic constants viz, diffraction Young's modulus and X-ray elastic constant. It is observed that within the Stokes-Wilson formalism the appropriately normalized ratio of Diffraction elastic constant ratio (DER) or XEC ratio is capable of rationalizing the observed broadening anisotropy in the generalized Williamson-Hall plot with a suitable scaling parameter,  $\chi$  or  $\sqrt{\chi}$  as the case may be. For prominent dislocation-induced line broadening or non-uniform microstrain (for deformed Cu sample) a scaling parameter of  $\sqrt{\chi}$  provides better estimates of crystallite size and microstrain. This new method is an improvement over the work of Jiang et al. which is based on uniform microstrain, while in the present work non-uniform microstrains, which are present in dislocated crystals, can be adequately taken into account. It is observed that elastic grain interaction models such as Reuss, Reuss-Voigt average have a profound influence on the line broadening anisotropy. The method was successfully applied on two model systems Aluminum and Copper (which differs considerably in their elastic anisotropy) which were deformed in various modes, namely cold-working (filing), cold-rolling and ball milling. The present method provides values for crystallite size and lattice microstrain that are well comparable with literature values. In the case of deformed powder materials, the Reuss-model offers a much better fit than the Reuss-Voigt model. Both models provide identical results for Al in bulk deformed material. The anisotropy corrected Williamson-Hall plot is not linear for heavily deformed materials, indicative of dislocation induced line broadening. The method is simple and can be applied to FCC crystal systems. The method can overcome the assumptions involved in modified-Williamson-Hall /modified Warren-Averbach method or its variants to rationalize line broadening anisotropy.

#### Conflict of interest statement

The authors declare that they have no conflict of interest.

## References

- [1] H. P. Klug and L. E. Alexander. *X-ray diffraction procedures: for polycrystalline and amorphous materials*. John Wiley and Sons, 2nd edition, 1974.
- [2] B. E. Warren. *X-ray Diffraction*. Dover Publication Inc., 1st edition, 1990.

- [3] B. E. Warren and B. L. Averbach. *J. Appl. Phys.*, **23**:497, 1952.
- [4] G. K. Williamson and W. H. Hall. *Acta Metallurgica*, **1**:22, 1953.
- [5] N. C. Halder and C. N. J. Wagner. *Acta Cryst*, **20**:312, 1966.
- [6] P. Chatterjee and S. P. Sen Gupta. *J. Appl. Cryst.*, **32**:1060, 1999.
- [7] T. Ungar and A. Borbely. *Appl. Phys. Lett.*, **69**:3173, 1996.
- [8] A. R. Stokes and A. J. C. Wilson. *Proc. Physical Society*, **56**:174, 1944.
- [9] B. Clausen, T. Lorentzen, and T. Leffers. *Acta Mater.*, **46**:3087, 1998.
- [10] A. K. Singh and C. Balasingh. *J. Appl. Phys.*, **90**:2296, 2001.
- [11] C. C. Tang, P. A. Lynch, R. W. Cheary, and S. M. Clark. *J. Appl. Cryst.*, **40**:642, 2007.
- [12] D. Rafaja, C. Krbetschek, C. Ullrich, and S. Martin. *J. Appl. Cryst.*, **47**:936, 2014.
- [13] S. R. Agnew, A. Singh, C. A. Calhoun, R. P. Mulay, J. J. Bhattacharyya, H. Somekawa, T. Mukai, B. Clausen, and P.D. Wu. *Int. J. Plasticity*, **100**:34, 2018.
- [14] S. D. Bakshi, D. Sinha, and S. G. Chowdhury. *Mater. Character.*, **142**:144, 2018.
- [15] A. K. Chandan, G. Mishra, B. Mahato, S. G. Chowdhury, S. Kundu, and J. Chakraborty. *Metall. Mater. Trans. A*, **50**:4851, 2019.
- [16] F. Jiang, T. Masumura, K. Hirata, T. Tsuchiyama, and S. Takaki. *Int. J. Plasticity*, **112**:89, 2019.
- [17] P. W. Stephens. *J. Appl. Cryst.*, **32**:281, 1999.
- [18] N. C. Popa. *J. Appl. Cryst.*, **31**:176, 1998.
- [19] J. Rodriguez-Carvajal. *IUCr Newsletter*, **26**:12, 2001.
- [20] B. H. Toby and R. B. Von Dreele. *J. Appl. Cryst.*, **46**:544, 2013.
- [21] M. Wilkens. *Physica Stat. Solid.A*, **2**:359, 1970.
- [22] G. Ribarik, T. Ungar, and J. Gubicza. *J. Appl. Cryst.*, **34**:669, 2001.
- [23] G. Ribarik, B. Joni, and T. Ungar. *Crystals*, **10**:623, 2020.
- [24] W. H. Hall. *Proc. Physical Soc. Sec A*, **62**:741, 1949.
- [25] J. H. Auld and R. I. Garrod. *Nature*, **169**:579, 1952.
- [26] L. M. Zhao and Z.D. Zhang. *Scripta Mater.*, **58**:283, 2008.
- [27] S. L. Wong and P. R. Dawson. *Acta Mater.*, **58**:1658, 2010.
- [28] S. Takaki, F. Jiang, T. Masumura, and T. Tsuchiyama. *ISIJ International*, **58**:769, 2018.
- [29] M. K. A. Koker, U. Welzel, and E. J. Mittemeijer. *Phil. Mag.*, **93**:2967, 2013.
- [30] M. K. A. Koker, U. Welzel, and E. J. Mittemeijer. *J. Appl. Cryst.*, **47**:391, 2014.
- [31] W. Voigt. *Lehrbuch der Kristallographie*, **34**:964, 1910.
- [32] A. Reuss. *Zeitschrift Fur Angewandte Mathematik Und Mechanik*, **9**:49, 1929.
- [33] H. Neerfeld. *Mitt. Kaiser-Wilhelm. Inst. Eisenforsch.*, **24**:61, 1942.
- [34] R. Hill. *Proc. Physical Soc. Sec. A*, **65**:349, 1952.
- [35] J. D. Eshelby. *Proc. Royal Soc. A: Math. Phys. Sci.*, **241**:376, 1957.
- [36] E. Kroner. *J. Phys.*, **151**:504, 1958.
- [37] U. Welzel, J. Ligot, P. Lamparter, A. C. Vermeulen, and E. J. Mittemeijer. *J. Appl. Cryst.*, **38**:1, 2005.
- [38] P. Scherrer. *Nachr. Ges. Wiss. Gottingen*, **2**:98, 1918.
- [39] T. Ungar, J. Gubicza, G. Ribarik, and A. Borbely. *J. Appl. Cryst.*, **34**:298, 2001.
- [40] T. Ungar and G. Tichy. *Physica Stat. Solid.A*, **171**:425, 1999.
- [41] I. C. Noyan and J. B. Cohen. *Determination of strain and stress fields by diffraction methods (in Residual Stress)*. Springer, 1th edition, 1987.
- [42] M. T. Hutchings, P. J. Withers, T. M. Holden, and T. Lorentzen. *Introduction to the Characterization of Residual Stress by Neutron Diffraction*. CRC Press, 1th edition, 2005.
- [43] M. Casas-Cabanas, M. Reynaud, J. Rikarte, P. Horbach, and J. Rodriguez-Carvajal. *J. Appl. Cryst.*, **49**:2259, 2016.
- [44] P. Thompson, D. E. Cox, and J.B. Hastings. *J. Appl. Cryst.*, **20**:79, 1987.
- [45] Th. H. de Keijser, J. I. Langford, E. J. Mittemeijer, and A. B. P. Vogels. *J. Appl. Cryst.*, **15**:308, 1982.
- [46] C. N. J. Wagner. *Local atomic arrangements studies by X-ray diffraction*. Gordon and Breach Science Publishers Inc., 1th edition, 1966.
- [47] T. Ungar, A. Revesz, and A. Borbely. *J. Appl. Cryst.*, **31**:554, 1998.
- [48] T. Berecz. *Mat. Sci. Tech.*, **35**:513, 2019.

- [49] J. Gubicza, N. H. Nama, L. Balogh, R. J. Hellmiga, V. V. Stolyarov, Y. Estrin, and T. Ungar. *J. Alloy. Comp.*, **378**:248, 2004.
- [50] G. Csizar, L. Balogh, A. Mishra, X. Zhang, and T. Ungar. *J. Appl. Phys.*, **110**:043502, 2011.
- [51] M. Mojtahedi, M. Goodarzi, M. R. Aboutalebi, and V. Soleimani. *Powd.Diffra.*, **30**:14, 2015.
- [52] S. N. Dey, P. Chatterjee, and S. P. Sengupta. *J. Phys. D: Appl. Phys.*, **38**:1444, 2005.
- [53] A. L. Ortiz and L. Shaw. *Acta Mater.*, **52**:2185, 2004.
- [54] A. S. Khan, B. Farrokh, and L. Takacs. *Mat. Sci. Eng. A*, **489**:77, 2008.
- [55] P. Guyot and G. M. Raynaud. *Acta Metallurgica Mater.*, **39**:317, 1991.
- [56] S. S. Satheesh Kumar and T. Raghu. *Mater. Design*, **57**:114, 2014.